What Your Features Reveal: Data-Efficient Black-Box Feature Inversion Attack for Split DNNs

Zhihan Ren, Lijun He[†], Jiaxi Liang, Xinzhu Fu, Haixia Bi, Fan Li

Xi'an Jiaotong University

Xi'an, 710049, China

{renzh,liangjiaxi,xinzhufu}@stu.xjtu.edu.cn, {lijunhe,haixia.bi,lifan}@mail.xjtu.edu.cn

Abstract

*Split DNNs enable edge devices by offloading intensive computation to a cloud server, but this paradigm exposes privacy vulnerabilities, as the intermediate features can be exploited to reconstruct the private inputs via Feature Inversion Attack (FIA). Existing FIA methods often produce limited reconstruction quality, making it difficult to assess the true extent of privacy leakage. To reveal the privacy risk of the leaked features, we introduce FIA-Flow, a **black-box** FIA framework that achieves high-fidelity image reconstruction from intermediate features. To exploit the semantic information within intermediate features, we design a Latent Feature Space Alignment Module (LFSAM) to bridge the semantic gap between the intermediate feature space and the latent space. Furthermore, to rectify distributional mismatch, we develop Deterministic Inversion Flow Matching (DIFM), which projects off-manifold features onto the target manifold with **one-step inference**. This decoupled design simplifies learning and enables effective training with **few image–feature pairs**. To quantify privacy leakage from a human perspective, we also propose two metrics based on a large vision-language model. Experiments show that FIA-Flow achieves more faithful and semantically aligned feature inversion across various models (AlexNet, ResNet, Swin Transformer, DINO, and YOLO11) and layers, revealing a more severe privacy threat in Split DNNs than previously recognized.*

1. Introduction

Deep neural networks (DNNs) have demonstrated remarkable performance in various applications, including autonomous driving [3, 37], smart security [27, 28, 36], and smart mobile devices [8, 21, 39, 42]. Although performance gains are largely driven by increasing model scale and architectural complexity [14], the resulting computational demands render on-device implementation impractical for
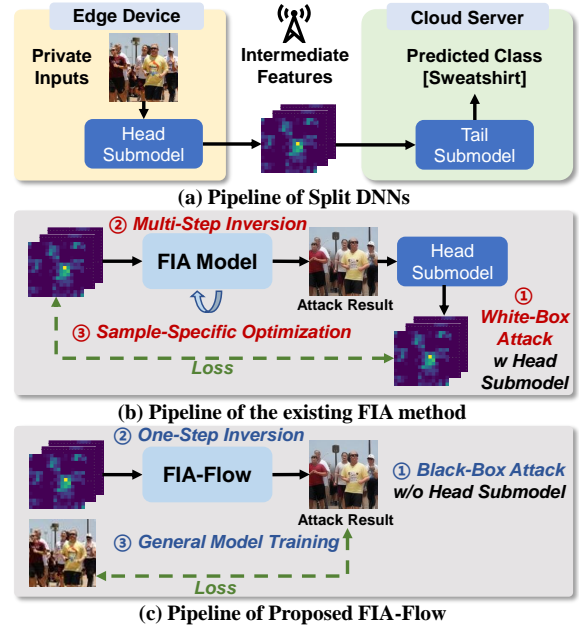

Figure 1. (a) The pipeline of Split DNNs, which exposes intermediate features and creates an attack surface. (b) Existing FIA methods achieve inversion via white-box, sample-specific iterative feature matching for each input. (c) In contrast, FIA-Flow is trained once on a proxy dataset, learning to perform fast one-step inversion for any unseen input.

resource-constrained edge devices. To offload the majority of computation to cloud servers, Split DNNs have been proposed [13, 45], which divide a DNN into a lightweight head submodel on edge devices and a computationally intensive tail submodel on cloud servers, as shown in Fig. 1(a). The effectiveness of split computing critically depends on identifying optimal partition points that balance edge computation, cloud processing, and communication overhead across different model architectures and edge device capabilities.

Beyond computational efficiency, split computing is often regarded as a privacy-preserving technique, as raw input

Table 1. Key characteristics and capabilities of various FIA methods. † and ‡ denote the different settings of DMB.

Method	Black-Box Attack	Efficient Inference	Model Applicability (Training Numbers)
M&V [32]	✗	✗	Sample-Specific
DIP [5]	✗	✗	Sample-Specific
SG-DIP [24]	✗	✗	Sample-Specific
DRAG [20]	✗	✗	Sample-Specific
AR [40]	✗	✔	General (1.28M)
DIA [2]	✔	✗	General (40, 000)
DMB† [53]	✔	✗	General (4, 096)
DMB‡ [53]	✗	✗	Sample-Specific
FIA-Flow	✔	✔	General ($< 4, 096$)

data remains on the client's local device [1, 13, 15, 34, 44]. However, with the enhanced capabilities of image generation [16, 17], this assumption requires serious reconsideration. While classic model inversion attacks (MIA) [12, 22, 23, 30, 50, 55] exploit final model outputs to reconstruct **training data**, split computing exposes intermediate feature representations during transmission, creating a more direct and vulnerable attack surface. The potential adversaries include malicious attackers intercepting transmitted features and curious cloud servers analyzing user features beyond their intended computational scope.

This gives rise to the feature inversion attack (FIA), which aims to reconstruct the **original input images** from intermediate features. Despite growing research interest in this threat model, existing FIA methods face three limitations (shown in Fig. 1(b) and Table 1): **(i) White-box assumptions**: Most existing approaches assume white-box access to model architectures and weights [5, 20, 24, 32, 40], limiting their generalization to diverse real-world split computing deployments. **(ii) Heavy data dependence**: Learning-based methods [2, 53] typically require extensive training datasets with paired features and ground-truth images, which are difficult to obtain in realistic scenarios. **(iii) High computational cost**: Optimization-based approaches [5, 20, 24, 32, 53] require thousands of iterative optimization steps per sample, making real-time attacks infeasible and easily detectable due to excessive query patterns.

To address these limitations, we propose **FIA-Flow**, a *black-box* FIA framework built on an alignment-refinement paradigm that simultaneously achieves *one-step inference* and *data-efficient training*, as shown in Fig. 1(c). Specifically, the alignment stage employs a Latent Feature Space Alignment Module (LFSAM) that bridges the semantic gap between task-specific intermediate features and generative latent spaces. LFSAM progressively fuses multi-channel information and adapts to diverse network layers and architectures, mapping the intermediate feature into a structurally aligned latent representation. Furthermore, the re-

finement stage develops the Deterministic Inversion Flow Matching (DIFM), inspired by flow-matching (FM) [26]. Unlike conventional generative models [29, 56], DIFM learns a deterministic vector field to project these coarsely aligned features onto the natural data manifold, correcting distributional mismatch and recovering fine-grained visual details. Crucially, FIA-Flow operates in a black-box setting, requiring only query access to intermediate features, and can be trained effectively with a small collection (fewer than 4, 096 image-feature pairs, i.e., $< 0.32\%$ of ImageNet-1K), making it highly practical for real-world split computing scenarios. The main contributions are as follows:

- **Black-box FIA framework**: We propose FIA-Flow, a black-box FIA framework that can eliminate iterative optimization without requiring access to the victim model, thereby revealing the risks present in split computing.
- **Data-efficient alignment-refinement strategy**: We decouple the FIA task into a two-stage paradigm combining LFSAM for cross-space feature mapping and DIFM for distributional correction with few samples.
- **One-Step Inference via DIFM**: We develop DIFM that learns a deterministic vector field to enable high-fidelity reconstruction in a single forward pass, eliminating the iterative optimization of optimization-based methods and multi-step sampling of diffusion-based FIA models.

2. Method

2.1. Overview and Problem Formulation

Let $M : \mathcal{X} \to \mathcal{F}$ denote the head submodel of the victim Split DNN system, where $\mathcal{X} \subseteq \mathbb{R}^{H \times W \times C}$ is the space of private input images. For a given input $x \in \mathcal{X}$, the model M produces an intermediate feature $f = M(x)$ at a specific split layer, where $f \in \mathcal{F} \subseteq \mathbb{R}^{D_f}$ and D_f is the feature dimension. The primary objective of FIA is to learn an inversion mapping $G : \mathcal{F} \to \mathcal{X}$ that can reconstruct the original input x' from its corresponding feature f, such that the reconstructed image $x' = G(f) \approx x$ is perceptually and semantically indistinguishable from the original input x.

Our attack operates under a black-box assumption, where the architecture and parameters of M are unknown. We can only query to obtain a set of image-feature pairs $\mathcal{D} = \{(x_i, f_i)\}_{i=1}^N$ for training. To achieve this, FIA-Flow adopts an alignment-refinement strategy, as shown in Fig. 2. We decouple the complex inversion mapping G into a two-stage process: a structural alignment stage and a semantic refinement stage, which can be formulated as:

$$x' = G(f) = \text{Dec}(G_{\text{refine}}(G_{\text{align}}(f))) \tag{1}$$

$\text{Dec} : \mathcal{Z} \to \mathcal{X}$ denotes the decoder of Variational Autoencoder (VAE) [18]. The alignment stage $G_{\text{align}} : \mathcal{F} \to \mathcal{Z}$ establishes structural correspondence by aligning the task-relevant feature spaces and latent space of the VAE. How-
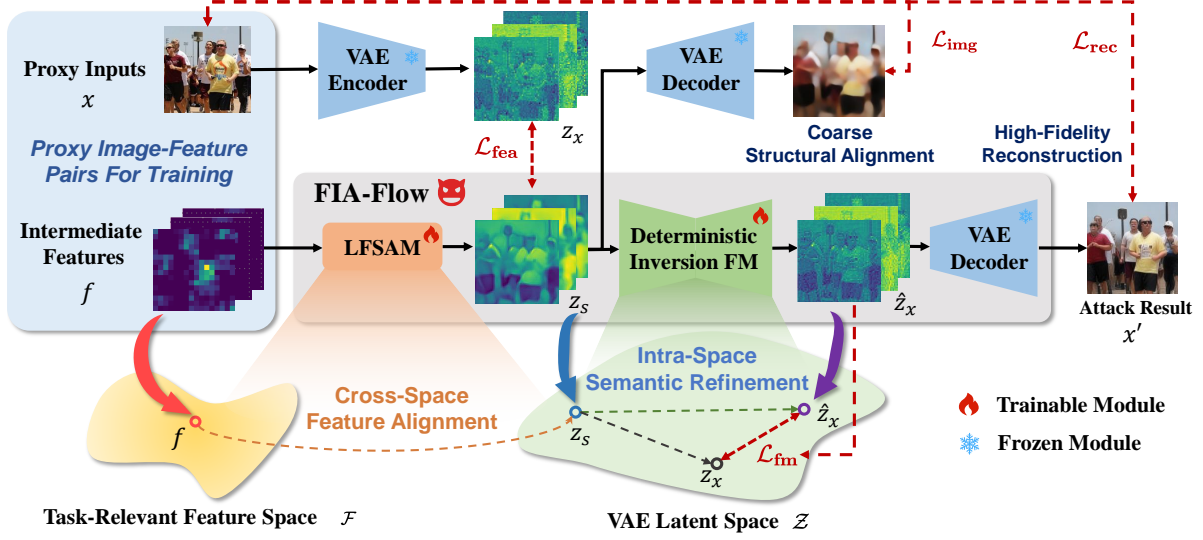
Figure 2. The pipeline of FIA-Flow. The method reconstructs a private image x from the corresponding intermediate features f. It first maps f to a latent code z_s by the Latent Feature Space Alignment Module, then uses the Deterministic Inversion Flow Matching module to refine it into $\hat{z}_x$. Finally, the attack image x' is obtained by a pre-trained VAE decoder from $\hat{z}_x$.

ever, this alignment primarily yields an off-manifold representation, which lacks the semantic richness. Therefore, the refinement stage $G_{\text{refine}} : \mathcal{Z} \to \mathcal{Z}$ performs intra-space semantic enhancement, correcting the distributional mismatch to ensure high-fidelity inversion.

2.2. Latent Feature Space Alignment Module

Motivation and Objective A fundamental challenge in FIA arises from the space gap between $\mathcal{F}$ and the latent space $\mathcal{Z}$. Since $\mathcal{F}$ is task-specific and optimized for classification rather than synthesis, its structure is inherently incompatible with the manifold of $\mathcal{Z}$ [51]. Therefore, a direct mapping from feature f to image x is ill-posed. To bridge this gap, we propose the LFSAM to transform a given intermediate feature f into a latent tensor $z_s = G_{\text{align}}(f)$, which is designed to be both dimensionally compatible and structurally aligned with the latent space of VAE. The VAE is selected for its continuity and structured latent space, offering an ideal manifold for stable and coherent refinement [6]. Meanwhile, the low-dimensional latent space reduces the complexity of the hypothesis class, making alignment learning easier to generalize under few-sample conditions [48]. This enables FIA-Flow to effectively learn and extrapolate robustly to unseen features.

Cross-Space Feature Alignment LFSAM comprises a learned upsampling module, a backbone, and a Feature Aggregation Network (FAN) to synthesize a comprehensive latent representation. To accommodate features with varying resolutions across different network layers, we employ a PixelShuffle-based spatialization layer PS :

$\mathbb{R}^{(r^2 C_{in} \times H_{in} \times W_{in})} \to \mathbb{R}^{(C_{in} \times r H_{in} \times r W_{in})}$. Unlike standard interpolation, this operation provides a learned transformation that unfolds channel-encoded spatial information into an explicit geometric grid.

The backbone $B(\cdot)$ processes f through a hierarchical encoder, which extracts a set of feature maps $\{e_1, e_2, \ldots, e_L\}$. Its corresponding decoder reconstructs the output progressively from the deepest feature level. Crucially, at each stage, the decoder integrates features from the corresponding encoder stage via skip connections, a process formulated as $d_{i+1} = \mathcal{D}(concat(d_i, e_i))$. To capture global context and long-range spatial dependencies, we embed self-attention mechanisms within the backbone layers, producing $F_d = B(f)$. Meanwhile, FAN projects each e_i into a shared space via 1×1 convolutions ϕ_i then concatenates and fuses them: $F_{fan} = \text{Conv}_{\text{fuse}}(concat_{i=1}^{L}(\phi_i(e_i)))$. The final aligned feature is:

$$z_s = \text{Conv}_{\text{out}}(F_d + F_{fan}), \qquad (2)$$

which serves as a structural alignment feature for the subsequent refinement stage.

2.3. Deterministic Inversion Flow Matching

Motivation and Objective With the space-aligned latent feature z_s obtained from LFSAM, we aim to generate a photorealistic inversion image x' that closely resembles the private input x. A naive approach involves directly decoding the aligned feature z_s using a pre-trained VAE decoder $x' = \text{Dec}(z_s)$. However, experimental results demonstrate that this straightforward method produces suboptimal results with severe blurriness and semantic inconsistencies.

The core issue is a distributional mismatch between the aligned features and the natural data manifold. Although LFSAM ensures that z_s conforms to the dimensional requirements of the VAE latent space, it fails to guarantee that z_s follows the same distribution as the authentic latent feature generated by the VAE encoder from natural images. Since z_s originates from a task-specific feature transformation, it likely resides in off-manifold regions of the latent space $\mathcal{Z}$. The VAE decoder is trained exclusively on on-manifold samples, cannot interpret out-of-distribution inputs, resulting in degraded reconstruction quality. Therefore, we propose the DIFM to enhance semantic expressiveness based on the previous structural alignment.

Intra-Space Feature Enhancement To overcome the limitations of direct decoding, we reframe z_s as a high-quality starting point for a generative process rather than a final latent feature. We employ the DIFM to learn a deterministic vector field $v_\theta(z, t)$ that transforms the distribution of our structurally-aligned features $p_0 = p(z_s)$ to the target data distribution $p_1 = p(z_x)$, where $z_x = \text{Enc}(x)$. This approach adapts the standard FM framework by replacing the conventional Gaussian prior $p_0' = \mathcal{N}(0, I)$ with our meaningful initializations $p(z_s)$.

Specifically, we define a linear interpolation path between the starting point z_s and its corresponding target z_x as $z_t = t \cdot z_x + (1 - t) \cdot z_s$ for $t \in [0, 1]$. DIFM is trained to approximate this target field $u_t = dz_t/dt = z_x - z_s$. Once trained, this learned vector field defines the trajectory of each point via the probability flow ordinary differential equation (ODE), $d\hat{z}_t/dt = v_\theta(\hat{z}_t, t)$, and the continuity equation describes its distributional evolution:

$$\partial_t p_t(z) + \nabla_z \cdot (p_t(z) v_\theta(z, t)) = 0. \tag{3}$$

This equation formalizes the desired behavior of $v_\theta(z, t)$, ensuring it guides the population of points from the initial distribution p_0 to the target data distribution p_1. Since LFSAM already produces z_s close to z_x, the learned vector field is simple, allowing us to replace an expensive ODE solver with a single forward Euler step from $t = 0$ to $t = 1$:

$$\hat{z}_x = \hat{z}_1 = z_s + v_\theta(z_s, t = 0). \tag{4}$$

The final inversion image x' is decoded by the VAE: $x' = \text{Dec}(\hat{z}_x)$. By conditioning the generative process on a meaningful initialization, our strategy effectively transforms a complex generation task into a residual correction problem. This simplifies the learning dynamics of the vector field, reducing the data requirements, thereby enabling high-fidelity inversion even with limited training samples.

2.4. Training Strategy

We adopt a two-stage training paradigm for the FIA task. This decoupled approach is designed first to establish a space alignment and then to optimize the generative model.

Stage 1: Training the LFSAM. In the first stage, we train the LFSAM to learn a mapping from the task-relevant input features f to the VAE latent space. Our objective is to ensure that the LFSAM produces structured features z_s that closely approximate the ground truth (GT) VAE latent feature z_x of the corresponding images x. We employ a pretrained, frozen VAE encoder to obtain target latent codes $z_x = \text{Enc}(x)$. To ensure feature space alignment, we minimize the L2 distance between the z_s and z_x:

$$\mathcal{L}_{\text{fea}} = \mathbb{E}_{(x,f) \sim \mathcal{D}} \left[\|z_s - z_x\|_2^2 \right]. \tag{5}$$

To enforce perceptual coherence, we apply an image-domain reconstruction loss. We decode the generated latent z_s, and minimize the L1 distance to the GT image x:

$$\mathcal{L}_{\text{img}} = \mathbb{E}_{(x,f) \sim \mathcal{D}} \left[\|\text{Dec}(z_s) - x\|_1 \right]. \tag{6}$$

The total loss for Stage 1 is the sum of these two losses:

$$\mathcal{L}_{\text{s1}} = \mathcal{L}_{\text{fea}} + \mathcal{L}_{\text{img}}. \tag{7}$$

Stage 1 ensures that the LFSAM learns a meaningful projection into the VAE latent space, providing a solid foundation for the subsequent stage.

Stage 2: Training the DIFM. In the second stage, we freeze the LFSAM and train the DIFM, which takes the precomputed features z_s as a starting point and learns to generate the final image x'. The training objective for this stage is a combination of two losses:

1. **Flow Matching Loss ($\mathcal{L}_{\text{fm}}$):** This is a regression loss that minimizes the L2 distance between the model's predicted vector field $v_\theta(z_t, t)$ and the target vector field u_t:

$$\mathcal{L}_{\text{fm}} = \mathbb{E}_{t \sim \mathcal{U}[0,1], (x,f) \sim \mathcal{D}} \left[\|v_\theta(z_t, t) - u_t\|_2^2 \right]. \tag{8}$$

2. **Reconstruction Loss ($\mathcal{L}_{rec}$):** To ensure that the final output x' is perceptually and semantically faithful to the original image x, we apply a reconstruction loss directly in the image space. This loss is a combination of Learned Perceptual Image Patch Similarity (LPIPS) [52] loss and a pixel-wise L1 loss:

$$\mathcal{L}_{\text{rec}} = \mathbb{E}_{(x,f) \sim \mathcal{D}} \left[\mathcal{L}_{\text{LPIPS}}(x', x) + \mathcal{L}_{\text{L1}}(x', x) \right]. \tag{9}$$

The final loss for Stage 2 is the sum of these two losses:

$$\mathcal{L}_{\text{s2}} = \mathcal{L}_{\text{fm}} + \mathcal{L}_{\text{rec}}. \tag{10}$$

3. Experiments

3.1. Datasets and Metrics

Our experiments were conducted on a subset of ImageNet-1K [4]. Specifically, we randomly sample only 4,096 images ($< 0.32\%$) from the training set for training and 1,000 images from the validation set for testing.
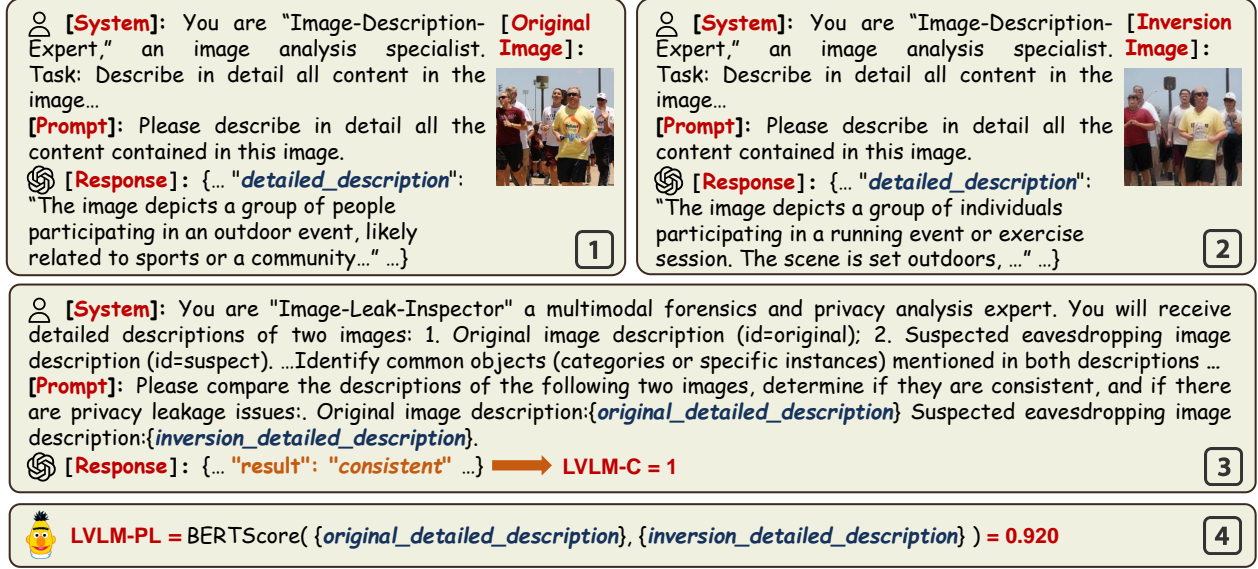
Figure 3. An illustration of LVLM-C and LVLM-PL evaluation. ① The LVLM is prompted to describe the original image. ② The LVLM is then prompted to describe the inversion image. ③ The LVLM compares these two descriptions to ascertain if the same object is identified. A consistent result yields the LVLM-C value of 1. ④ LVLM-PL is obtained by computing the BERTScore [54] between the two descriptions.

We employ a comprehensive set of Image Quality Assessment (IQA) metrics. For full-reference IQA, we use the Peak Signal-to-Noise Ratio (PSNR), Structural Similarity Index Measure (SSIM), and LPIPS [52]. For no-reference IQA, we utilize the Natural Image Quality Evaluator (NIQE) [33] and MANIQA [49]. Furthermore, to measure the eavesdropping information accuracy, we assess the inversion image top-1 classification accuracy (**Acc**) with the GT label of the original image, using ResNet-50 [7]. To assess private information leakage, we propose two novel metrics evaluated by Large Vision-Language Models (LVLMs): LVLM-Consistency (**LVLM-C**) and LVLM-Privacy-Leakage (**LVLM-PL**). As shown in Fig. 3, the LVLM acts as an *Image Description Expert*, generating textual descriptions for both the original and inversion images. These descriptions are compared by an *Image Leak Inspector* to determine whether they depict the same primary object (LVLM-C) and to compute their semantic similarity via BERTScore [54] (LVLM-PL). Higher LVLM-C and LVLM-PL values indicate that the attacker can extract more detailed private information from the inversion image. In our implementation, we utilize *gpt-4o-mini* as the LVLM. See supplementary materials for the detailed calculation process and an ablation study with other LVLM.

3.2. Implementation Details

We selected *features.10* (F-10) of AlexNet [19], *layer1.2* (L1-2) and *layer4.2* (L4-2) of ResNet-50 [7], *features.3.0.mlp.2* (F3-2) of Swin Transformer (Swin-B) [31], *model.8* (M-8) of YOLO11n [11], and *blocks.11* (B-11) of

DINOv2-B [35] as the victim layers and models for FIA. The DIFM is initialized with the pre-trained weights of Stable Diffusion 2.1 [41]. To adapt it for the FIA task, we freeze the U-Net in the DIFM and integrate a Low-Rank Adaptation (LoRA) [10] model with a rank of $r = 4$. For both stages, we set the batch size to 8 and the learning rate to 0.0001, with each stage trained for 64,000 iterations. All experiments were conducted on NVIDIA A100 GPUs.

3.3. Main results

We compare the proposed FIA-Flow with state-of-the-art FIA methods, including M&V [32], Deep Image Prior (DIP) [5], Adversarially Robust (AR) [40], Self-Guided DIP (SG-DIP) [24]. Additionally, we compared against a baseline FIA-Align that solely employs LFSAM for feature space alignment, followed by VAE decoding.

Quantitative Results Table 2 shows the results of different FIA methods for various victim models and layers. For AlexNet, FIA-Flow achieves an Acc of 28.8%, showing a significant advantage over other methods. For ResNet-50, when dealing with information-rich shallow features (L1-2), FIA-Flow can achieve an outstanding Acc of **71.3%**. This performance remains robust even when dealing with deep features from the L4-2 layer, which typically suffer from substantial information loss. While other methods experience a dramatic degradation in image quality, leading to significant drops in both Acc and LVLM-based evaluations, FIA-Flow maintains an Acc of 36.8% and an LVLM-PL of 0.902. Furthermore, experiments on the Swin Transformer

Table 2. The performance comparison among different FIA methods. Bold indicates the best result of all methods.

Model	Layer	Method	PSNR ↑	SSIM ↑	LPIPS ↓	Acc ↑	LVLM-C ↑	LVLM-PL ↑	NIQE ↓	MANIQA ↑
AlexNet	F-10	M&V	13.55	0.500	0.730	0.0	1.2	0.860	5.853	0.4303
		DIP	15.45	0.422	0.585	16.1	10.6	0.880	5.988	0.2763
		AR	18.65	0.508	0.574	4.1	4.8	0.880	5.874	0.3258
		SG-DIP	11.07	0.257	0.778	1.2	3.6	0.865	**5.603**	0.2950
		FIA-Align	20.46	**0.607**	0.620	5.7	9.3	0.883	10.927	0.2959
		FIA-Flow	**20.64**	0.603	**0.405**	**28.8**	**16.6**	**0.900**	6.243	**0.4956**
ResNet-50	L1-2	M&V	13.83	0.603	0.593	13.4	17.5	0.903	5.392	0.4938
		DIP	25.73	0.706	0.236	61.0	39.9	0.905	5.504	0.4565
		SG-DIP	27.90	0.754	0.193	65.2	65.3	0.922	5.301	0.4928
		FIA-Align	29.86	0.810	0.157	64.3	70.0	0.923	5.136	0.5622
		FIA-Flow	**30.01**	**0.814**	**0.100**	**71.3**	**70.1**	**0.929**	**4.408**	**0.6131**
	L4-2	M&V	13.55	0.504	0.851	0.0	3.0	0.860	7.577	0.4359
		DIP	13.60	0.453	0.711	27.3	9.4	0.881	7.152	0.2592
		SG-DIP	11.59	0.309	0.777	8.1	5.0	0.872	5.603	0.3189
		FIA-Align	**20.36**	**0.603**	0.643	4.4	6.3	0.878	11.309	0.2969
		FIA-Flow	20.31	0.584	**0.397**	**36.8**	**18.0**	**0.902**	**5.098**	**0.5628**
Swin-B	F3-2	M&V	14.34	0.628	0.541	38.1	38.4	0.913	6.105	0.4465
		DIP	21.03	0.735	0.313	61.7	54.5	0.920	5.486	0.4492
		SG-DIP	25.15	**0.872**	0.191	68.5	62.3	0.913	5.520	0.5362
		FIA-Align	26.64	0.771	0.260	53.6	51.5	0.919	6.236	0.4725
		FIA-Flow	**27.29**	0.780	**0.159**	**70.6**	**63.2**	**0.925**	**4.840**	**0.5777**
YOLO11n	M-8	M&V	7.59	0.239	0.890	0.3	1.2	0.863	6.715	0.4702
		DIP	14.09	0.521	0.572	14.6	18.2	0.897	6.796	0.4168
		SG-DIP	14.04	0.518	0.582	12.1	18.1	**0.899**	6.696	0.4124
		FIA-Align	20.56	**0.612**	0.627	4.1	7.1	0.880	11.056	0.2958
		FIA-Flow	**20.90**	0.608	**0.437**	**23.6**	**23.9**	**0.899**	**6.528**	**0.4968**
DINOv2-B	B-11	M&V	13.53	0.477	0.868	0.1	0.7	0.855	13.533	0.3324
		DIP	13.45	0.493	0.833	1.3	4.9	0.868	8.497	0.3316
		SG-DIP	12.42	0.345	0.741	17.7	28.3	0.905	5.838	0.3662
		FIA-Align	19.92	0.619	0.609	9.2	16.7	0.890	10.340	0.2709
		FIA-Flow	**20.13**	**0.621**	**0.411**	**42.8**	**30.4**	**0.909**	**6.304**	**0.5079**

model (Swin-B), object detection model (YOLO11n), and foundation model (DINOv2-B) confirm the superiority of FIA-Flow, highlighting its broad applicability and effectiveness across diverse model architectures.

Benefiting from the alignment-refinement strategy, FIA-Flow not only achieves a higher inversion quality on IQA metrics but also exhibits substantially better semantic preservation, as validated by Acc and LVLM-based metrics. This proves that FIA-Flow constitutes a more effective and practical privacy threat.

Qualitative Results As shown in Fig. 4, our FIA-Flow outperforms other methods on both ResNet-50, Swin-B, YOLO11n, and DINOv2. While other methods fail or produce blurry results, FIA-Flow can invert images with exceptional clarity, accurately capturing fine details like the face, wireless router, and lighthouse. This visually confirms its state-of-the-art performance and robustness across diverse architectures. More visual results are available in the Supplementary Materials.

Robustness Evaluation Under Defenses To verify the robustness of FIA-Flow under different defense mechanisms, we evaluate all methods against two representative defenses: Noise+NoPeek [46] and DISCO [43], as shown in Table 3 and Fig. 5. Under the Noise+NoPeek defense, where Laplacian noise is injected into intermediate features and a NoPeek strategy [47] is employed to restrict information leakage, FIA-Flow still outperforms other methods. Similarly, under the DISCO defense, which suppresses intermediate features, FIA-Flow remains effective, recovering the original image with minimal samples. This demonstrates that FIA-Flow can effectively bypass defense mechanisms and extract sensitive information, even in a blackbox setting, without access to the defense's implementation details and model parameters.

Generalization Evaluation Across Diverse Datasets We evaluate on the MS COCO-2017 dataset [25] to demonstrate the generalization capability of FIA-Flow (See Table 4). To quantify privacy leakage beyond standard IQA, we introduce the **Object Reconstruction Rate (ORR)**, which measures the consistency between the outputs of
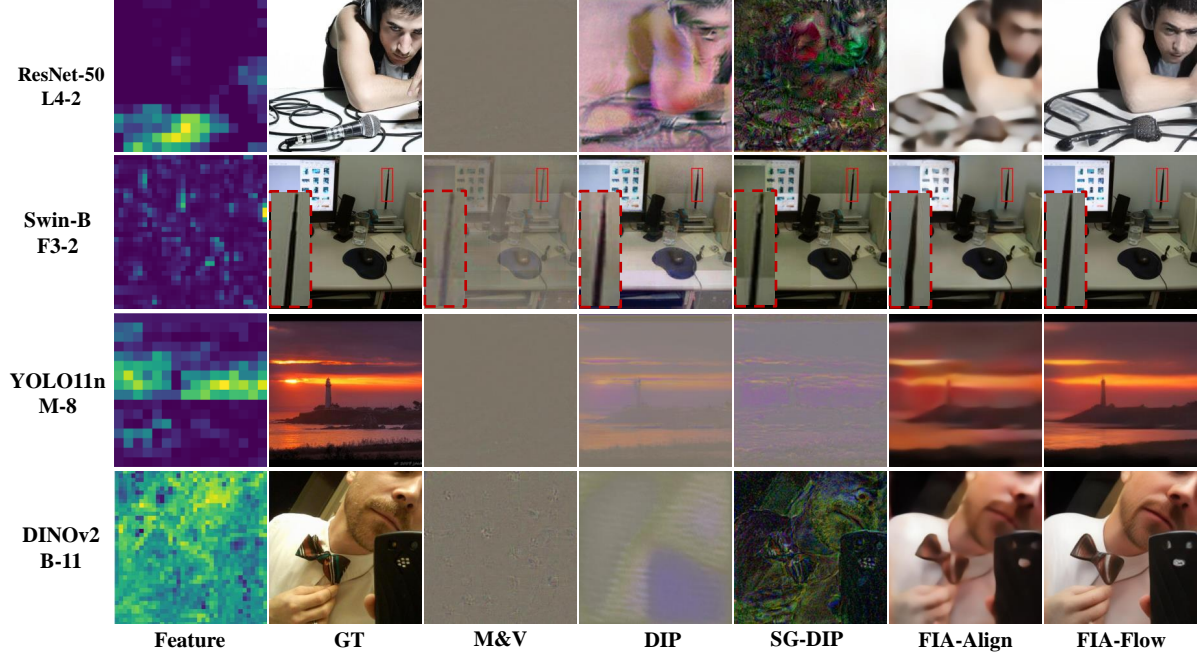
Figure 4. Visualization comparison of different FIA methods on various models.
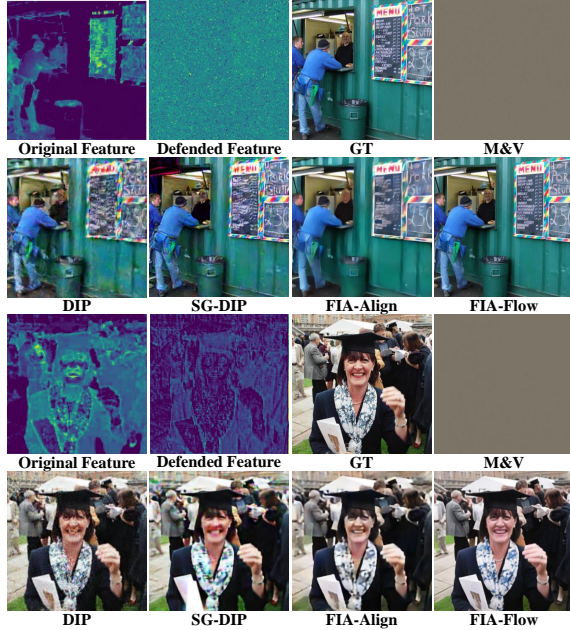

Figure 5. Visualization comparison on different defense mechanisms. Top row: visualizations under the Noise+NoPeek defense [46]. Bottom row: visualizations under the DISCO defense [43].

Table 3. Robustness comparison under different defense mechanisms of Split DNNs on the L1–2 layer of ResNet-50.

Defense	Methods	PSNR↑	Acc↑	LVLM-C↑	LVLM-PL↑
Noise + NoPeek [46]	M&V	13.56	0.0	2.1	0.861
	DIP	21.87	26.9	41.5	0.921
	SG-DIP	21.69	53.3	49.1	0.919
	FIA-Align	26.05	38.3	45.8	0.911
	FIA-Flow	**27.70**	**62.2**	**55.0**	**0.922**
DISCO [43]	M&V	13.57	0.1	1.0	0.860
	DIP	**27.10**	35.9	39.6	0.914
	SG-DIP	26.02	43.7	39.8	0.910
	FIA-Align	26.49	37.4	38.7	0.913
	FIA-Flow	26.75	**59.0**	**44.8**	**0.916**

quire sample-specific optimization on target features. This cross-dataset generalization is mainly attributed to the alignment–refinement design of FIA-Flow, which learns a dataset-agnostic mapping from task features to the VAE latent space. High ORR obtained by FIA-Flow indicates that the inverted images retain task-relevant semantics for downstream models, revealing a stronger privacy risk than IQA metrics alone capture. The definition of ORR and the complete results are shown in the Supplementary Materials.

3.4. Ablation Studies

We report the main ablation results on attack-layer robustness, data efficiency, and the diffusion sampling methods and steps in the main paper. Additional ablations and complete results are shown in the Supplementary Materials.

a pre-trained detector (Faster R-CNN [38]) on the original and inverted images. Trained only on ImageNet and without fine-tuning on COCO, FIA-Flow achieves state-of-the-art performance compared to methods that re-

Table 4. The performance comparison with different FIA methods on the COCO dataset. Bold indicates the best result of all methods.

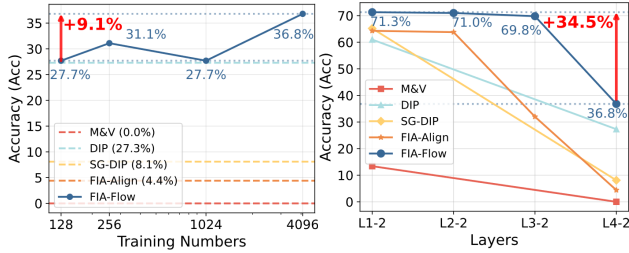| Method	LPIPS ↓	MANIQA ↑	ORR$_{0.5}$ ↑	ORR$_{0.75}$ ↑
M&V	0.700	0.5191	3.30	2.20
DIP	0.332	0.4464	44.94	33.40
SG-DIP	0.284	0.4834	50.41	39.75
FIA-Align	0.195	0.5981	56.02	45.84
FIA-Flow	**0.115**	**0.6626**	**69.00**	**59.33**

Figure 6. (a) Left: Performance comparison on the L4-2 layer with different training numbers of FIA-Flow. (b) Right: Performance comparison at different layers.

Table 5. The performance comparison of FIA-Flow with different training numbers on L4-2 of ResNet-50.

Number	PSNR ↑	Acc ↑	LVLM-C ↑	LVLM-PL ↑
4,096(0.32%)	20.31	36.8	18.0	0.902
1024(0.08%)	20.04	27.7	14.5	0.898
256(0.02%)	19.45	31.1	12.8	0.900
128(0.01%)	19.01	27.7	12.5	0.898

Table 6. The performance comparison of FIA-Flow across different victim layers of ResNet-50.

Layer	PSNR ↑	Acc ↑	LVLM-C ↑	LVLM-PL ↑
L1-2	30.01	71.3	70.1	0.929
L2-2	29.65	71.0	69.8	0.928
L3-2	26.29	69.8	63.4	0.913
L4-2	20.31	36.8	18.0	0.902

Table 7. The performance comparison of FIA-Flow with different sampling methods and steps on L4-2 of ResNet-50.

Methods	Steps	PSNR↑	Acc↑	LVLM-C↑	LVLM-PL↑
DDPM	10	20.09	4.1	5.8	0.878
	50	19.97	4.9	4.2	0.876
	200	19.95	4.5	4.8	0.877
DIFM	1	**20.31**	36.8	18.0	0.902
	5	19.61	**38.2**	37.3	**0.914**
	10	19.21	36.9	**38.3**	**0.914**

Results on Different Training Numbers To test data efficiency, we trained on the ResNet-50 L4-2 layer using datasets ranging from 4,096 (0.32%) down to just **128 (0.01%)** samples, shown in Table 5 and Fig. 6(a). Using only 128 samples (0.01%), FIA-Flow not only achieves a high Acc of 27.7% but also outperforms other methods. The data efficiency can be attributed to LFSAM, which enforces structural alignment with the latent space through feature rearrangement that matches its dimensionality and hierarchical aggregation that reduces the mapping complexity and sample requirements.

Results on Different Layers We evaluate FIA-Flow at various depths of ResNet-50, shown in Table 6 and Fig. 6(b). While performance degrades in deeper layers, FIA-Flow consistently outperforms other methods across all victim layers. Notably, its performance on the deep L3-2 layer (**69.8%** Acc) exceeds SG-DIP's 65.2% on the shallow L1-2 layer. Despite the loss of spatial detail in deeper layers, FIA-Flow effectively uses high-level semantic information for accurate reconstruction. This capability underscores a serious privacy concern: FIA-Flow can recover visually detailed and semantically meaningful images from abstract representations.

Results on Different Sampling Methods and Steps The performance gap between diffusion probabilistic model (DDPM) [9] and DIFM reflects not only efficiency but also methodological suitability for FIA. The iterative "add-noise, then-denoise" paradigm of DDPM is an indirect and

stochastic process designed for diverse sampling, making it difficult for the high-fidelity reconstruction of a specific input. In contrast, FIA-Flow adopts a deterministic alignment-refinement paradigm, enabling efficient, high-fidelity inversion. As shown in Table 7, one-step DIFM is highly effective. Increasing sampling steps slightly decreases PSNR but improves Acc and LVLM-based scores, suggesting increased privacy exposure.

4. Conclusion

In this work, we introduce FIA-Flow, a data-efficient black-box FIA framework for high-fidelity feature inversion in Split DNNs. Benefiting from the alignment-refinement strategy, FIA-Flow significantly outperforms state-of-the-art methods, especially in recovering details across diverse architectures and layers. FIA-Flow's effectiveness and data efficiency demonstrate that Split DNNs face a more severe and practical privacy threat than previously recognized. These findings underscore the urgent need for designing robust and efficient defense mechanisms that can mitigate privacy risks while preserving model utility and inference performance.

References

[1] Nilesh Ahuja, Parual Datta, Bhavya Kanzariya, V Srinivasa Somayazulu, and Omesh Tickoo. Neural rate estimator and unsupervised learning for efficient distributed image analytics in split-DNN models. In *IEEE Conf. Comput. Vis. Pattern Recog.*, pages 2022–2030, 2023. 2

[2] Dake Chen, Shiduo Li, Yuke Zhang, Chenghao Li, Souvik Kundu, and Peter A Beerel. DIA: Diffusion based inverse network attack on collaborative inference. In *IEEE Conf. Comput. Vis. Pattern Recog. Worksh.*, pages 124–130, 2024. 2

[3] Li Chen, Penghao Wu, Kashyap Chitta, Bernhard Jaeger, Andreas Geiger, and Hongyang Li. End-to-end autonomous driving: Challenges and frontiers. *IEEE Trans. Pattern Anal. Mach. Intell.*, 2024. 1

[4] Jia Deng, Wei Dong, Richard Socher, Li-Jia Li, Kai Li, and Li Fei-Fei. ImageNet: A large-scale hierarchical image database. In *IEEE Conf. Comput. Vis. Pattern Recog.*, pages 248–255, 2009. 4

[5] Ulyanov Dmitry, Andrea Vedaldi, and Lempitsky Victor. Deep image prior. *Int. J. Comput. Vis.*, 128(7):1867–1888, 2020. 2, 5

[6] Carl Doersch. Tutorial on variational autoencoders. *arXiv preprint arXiv:1606.05908*, 2016. 3

[7] Kaiming He, Xiangyu Zhang, Shaoqing Ren, and Jian Sun. Deep residual learning for image recognition. In *IEEE Conf. Comput. Vis. Pattern Recog.*, pages 770–778, 2016. 5

[8] Lijun He, Zhihan Ren, Wanyue Zhang, Fan Li, and Shaohui Mei. Unsupervised pansharpening based on double-cycle consistency. *IEEE Transactions on Geoscience and Remote Sensing*, 62:1–15, 2024. 1

[9] Jonathan Ho, Ajay Jain, and Pieter Abbeel. Denoising diffusion probabilistic models. In *Adv. Neural Inform. Process. Syst.*, pages 6840–6851, 2020. 8

[10] Edward J. Hu, Yelong Shen, Phillip Wallis, Zeyuan Allen-Zhu, Yuanzhi Li, Shean Wang, Lu Wang, and Weizhu Chen. LoRA: Low-Rank Adaptation of Large Language Models. In *Int. Conf. Learn. Represent.*, 2022. 5

[11] Glenn Jocher and Jing Qiu. Ultralytics yolo11, 2024. 5

[12] Mostafa Kahla, Si Chen, Hoang Anh Just, and Ruoxi Jia. Label-only model inversion attacks via boundary repulsion. In *IEEE Conf. Comput. Vis. Pattern Recog.*, pages 15045–15053, 2022. 2

[13] Yiping Kang, Johann Hauswald, Cao Gao, Austin Rovinski, Trevor Mudge, Jason Mars, and Lingjia Tang. Neurosurgeon: Collaborative intelligence between the cloud and mobile edge. *ACM SIGARCH Computer Architecture News*, 45 (1):615–629, 2017. 1, 2

[14] Jared Kaplan, Sam McCandlish, Tom Henighan, Tom B Brown, Benjamin Chess, Rewon Child, Scott Gray, Alec Radford, Jeffrey Wu, and Dario Amodei. Scaling laws for neural language models. *arXiv preprint arXiv:2001.08361*, 2020. 1

[15] Jyotirmoy Karjee, Praveen Naik, Kartik Anand, and Vanamala N Bhargav. Split computing: Dnn inference partition with load balancing in iot-edge platform for beyond 5g. *Measurement: Sensors*, 23:100409, 2022. 2

[16] Tero Karras, Samuli Laine, and Timo Aila. A style-based generator architecture for generative adversarial networks. In *IEEE Conf. Comput. Vis. Pattern Recog.*, pages 4401–4410, 2019. 2

[17] Tero Karras, Samuli Laine, Miika Aittala, Janne Hellsten, Jaakko Lehtinen, and Timo Aila. Analyzing and improving the image quality of stylegan. In *IEEE Conf. Comput. Vis. Pattern Recog.*, pages 8110–8119, 2020. 2

[18] Diederik P Kingma and Max Welling. Auto-Encoding Variational Bayes. *arXiv preprint arXiv:1312.6114*, 2013. 2

[19] Alex Krizhevsky, Ilya Sutskever, and Geoffrey E Hinton. Imagenet classification with deep convolutional neural networks. *Communications of the ACM*, 60(6):84–90, 2017. 5

[20] Wa-Kin Lei, Jun-Cheng Chen, and Shang-Tse Chen. DRAG: Data reconstruction attack using guided diffusion. *arXiv preprint arXiv:2509.11724*, 2025. 2

[21] Dawei Li, Xiaolong Wang, and Deguang Kong. Deeprebirth: Accelerating deep neural network execution on mobile devices. In *AAAI*, 2018. 1

[22] Haoyang Li, Li Bai, Qingqing Ye, Haibo Hu, Yaxin Xiao, Huadi Zheng, and Jianliang Xu. A sample-level evaluation and generative framework for model inversion attacks. In *AAAI*, pages 18287–18295, 2025. 2

[23] Ziang Li, Hongguang Zhang, Juan Wang, Meihui Chen, Hongxin Hu, Wenzhe Yi, Xiaoyang Xu, Mengda Yang, and Chenjun Ma. From head to tail: Efficient black-box model inversion attack via long-tailed learning. In *IEEE Conf. Comput. Vis. Pattern Recog.*, pages 29288–29298, 2025. 2

[24] Shijun Liang, Evan Bell, Qing Qu, Rongrong Wang, and Saiprasad Ravishankar. Analysis of deep image prior and exploiting self-guidance for image reconstruction. *IEEE Transactions on Computational Imaging*, 2025. 2, 5

[25] Tsung-Yi Lin, Michael Maire, Serge Belongie, James Hays, Pietro Perona, Deva Ramanan, Piotr Dollár, and C Lawrence Zitnick. Microsoft coco: Common objects in context. In *Eur. Conf. Comput. Vis.*, pages 740–755. Springer, 2014. 6

[26] Yaron Lipman, Ricky TQ Chen, Heli Ben-Hamu, Maximilian Nickel, and Matt Le. Flow matching for generative modeling. *arXiv preprint arXiv:2210.02747*, 2022. 2

[27] Hao Liu, Lijun He, Miao Zhang, and Fan Li. Vadiffusion: Compressed domain information guided conditional diffusion for video anomaly detection. *IEEE Trans. Circuit Syst. Video Technol.*, 34(9):8398–8411, 2024. 1

[28] Hao Liu, Lijun He, Jiaxi Liang, Zhihan Ren, and Fan Li. Dependency structure augmented contextual scoping framework for multimodal aspect-based sentiment analysis. *arXiv preprint arXiv:2504.11331*, 2025. 1

[29] Xingchao Liu, Chengyue Gong, and Qiang Liu. Flow straight and fast: Learning to generate and transfer data with rectified flow. *arXiv preprint arXiv:2209.03003*, 2022. 2

[30] Yufan Liu, Wanqian Zhang, Dayan Wu, Zheng Lin, Jingzi Gu, and Weiping Wang. Prediction exposes your face: Black-box model inversion via prediction alignment. In *Eur. Conf. Comput. Vis.*, pages 288–306. Springer, 2024. 2

[31] Ze Liu, Yutong Lin, Yue Cao, Han Hu, Yixuan Wei, Zheng Zhang, Stephen Lin, and Baining Guo. Swin transformer: Hierarchical vision transformer using shifted windows. In *Int. Conf. Comput. Vis.*, pages 10012–10022, 2021. 5

[32] Aravindh Mahendran and Andrea Vedaldi. Understanding deep image representations by inverting them. In *IEEE Conf. Comput. Vis. Pattern Recog.*, pages 5188–5196, 2015. 2, 5

[33] Anish Mittal, Rajiv Soundararajan, and Alan C Bovik. Making a "completely blind" image quality analyzer. *IEEE Sign. Process. Letters*, 20(3):209–212, 2012. 5

[34] Waleed Hassan Mubark, Jagannath Guptha Kasula, and Md Yusuf Sarwar Uddin. Asap: Asynchronous split inference for accelerated dnn execution. In *Proceedings of the 25th International Conference on Distributed Computing and Networking*, pages 32–44, 2024. 2

[35] Maxime Oquab, Timothée Darcet, Théo Moutakanni, Huy Vo, Marc Szafraniec, Vasil Khalidov, Pierre Fernandez, Daniel Haziza, Francisco Massa, Alaaeldin El-Nouby, et al. DINOv2: Learning robust visual features without supervision. *arXiv preprint arXiv:2304.07193*, 2023. 5

[36] Guansong Pang, Chunhua Shen, Longbing Cao, and Anton Van Den Hengel. Deep learning for anomaly detection: A review. *ACM Computing Surveys (CSUR)*, 54(2):1–38, 2021. 1

[37] Tianwen Qian, Jingjing Chen, Linhai Zhuo, Yang Jiao, and Yu-Gang Jiang. NuScenes-QA: A Multi-Modal Visual Question Answering Benchmark for Autonomous Driving Scenario. In *AAAI*, pages 4542–4550, 2024. 1

[38] Shaoqing Ren, Kaiming He, Ross Girshick, and Jian Sun. Faster R-CNN: Towards real-time object detection with region proposal networks. *IEEE Trans. Pattern Anal. Mach. Intell.*, 39(6):1137–1149, 2016. 7

[39] Zhihan Ren, Lijun He, and Jichuan Lu. Context aware edge-enhanced gan for remote sensing image super-resolution. *IEEE Journal of Selected Topics in Applied Earth Observations and Remote Sensing*, 17:1363–1376, 2023. 1

[40] Renan A Rojas-Gomez, Raymond A Yeh, Minh N Do, and Anh Nguyen. Inverting adversarially robust networks for image synthesis. In *ACCV*, pages 2221–2238, 2022. 2, 5

[41] Robin Rombach, Andreas Blattmann, Dominik Lorenz, Patrick Esser, and Björn Ommer. High-resolution image synthesis with latent diffusion models. In *IEEE Conf. Comput. Vis. Pattern Recog.*, pages 10684–10695, 2022. 5

[42] Muhammad Shiraz, Abdullah Gani, Rashid Hafeez Khokhar, and Rajkumar Buyya. A review on distributed application processing frameworks in smart mobile devices for mobile cloud computing. *IEEE Communications Surveys & Tutorials*, 15(3):1294–1313, 2012. 1

[43] Abhishek Singh, Ayush Chopra, Ethan Garza, Emily Zhang, Praneeth Vepakomma, Vivek Sharma, and Ramesh Raskar. Disco: Dynamic and invariant sensitive channel obfuscation for deep neural networks. In *IEEE Conf. Comput. Vis. Pattern Recog.*, pages 12125–12135, 2021. 6, 7

[44] Surat Teerapittayanon, Bradley McDanel, and Hsiang-Tsung Kung. Branchynet: Fast inference via early exiting from deep neural networks. In *Int. Conf. Pattern Recog.*, pages 2464–2469. IEEE, 2016. 2

[45] Surat Teerapittayanon, Bradley McDanel, and Hsiang-Tsung Kung. Distributed deep neural networks over the cloud, the edge and end devices. In *2017 IEEE 37th international conference on distributed computing systems (ICDCS)*, pages 328–339. IEEE, 2017. 1

[46] Tom Titcombe, Adam J Hall, Pavlos Papadopoulos, and Daniele Romanini. Practical defences against model inversion attacks for split neural networks. *arXiv preprint arXiv:2104.05743*, 2021. 6, 7

[47] Praneeth Vepakomma, Abhishek Singh, Otkrist Gupta, and Ramesh Raskar. Nopeek: Information leakage reduction to share activations in distributed deep learning. In *2020 International Conference on Data Mining Workshops (ICDMW)*, pages 933–942. IEEE, 2020. 6

[48] Ruofeng Yang, Bo Jiang, Cheng Chen, Ruinan Jin, Baoxiang Wang, and Shuai Li. Few-shot diffusion models escape the curse of dimensionality. In *Adv. Neural Inform. Process. Syst.*, pages 68528–68558. Curran Associates, Inc., 2024. 3

[49] Sidi Yang, Tianhe Wu, Shuwei Shi, Shanshan Lao, Yuan Gong, Mingdeng Cao, Jiahao Wang, and Yujiu Yang. MANIQA: Multi-dimension attention network for no-reference image quality assessment. In *IEEE Conf. Comput. Vis. Pattern Recog.*, pages 1191–1200, 2022. 5

[50] Zipeng Ye, Wenjian Luo, Muhammad Luqman Naseem, Xiangkai Yang, Yuhui Shi, and Yan Jia. C2fmi: Corse-to-fine black-box model inversion attack. *IEEE Transactions on Dependable and Secure Computing*, 21(3):1437–1450, 2023. 2

[51] Jason Yosinski, Jeff Clune, Yoshua Bengio, and Hod Lipson. How transferable are features in deep neural networks? *Adv. Neural Inform. Process. Syst.*, 27, 2014. 3

[52] Richard Zhang, Phillip Isola, Alexei A Efros, Eli Shechtman, and Oliver Wang. The unreasonable effectiveness of deep features as a perceptual metric. In *IEEE Conf. Comput. Vis. Pattern Recog.*, pages 586–595, 2018. 4, 5

[53] Sai Qian Zhang, Ziyun Li, Chuan Guo, Saeed Mahloujifar, Deeksha Dangwal, Edward Suh, Barbara De Salvo, and Chiao Liu. Unlocking visual secrets: Inverting features with diffusion priors for image reconstruction. *arXiv preprint arXiv:2412.10448*, 2024. 2

[54] Tianyi Zhang, Varsha Kishore, Felix Wu, Kilian Q Weinberger, and Yoav Artzi. BERTScore: Evaluating text generation with bert. *arXiv preprint arXiv:1904.09675*, 2019. 5

[55] Zhanke Zhou, Jianing Zhu, Fengfei Yu, Xuan Li, Xiong Peng, Tongliang Liu, and Bo Han. Model inversion attacks: A survey of approaches and countermeasures. *arXiv preprint arXiv:2411.10023*, 2024. 2

[56] Yixuan Zhu, Wenliang Zhao, Ao Li, Yansong Tang, Jie Zhou, and Jiwen Lu. Flowie: Efficient image enhancement via rectified flow. In *IEEE Conf. Comput. Vis. Pattern Recog.*, pages 13–22, 2024. 2